U.P.B. Sci. Bull., Series A, Vol. 87, Iss. 2, 2025 ISSN 1223-7027

PARTICLE STEERING SYSTEM FOR LASER-PLASMA ACCELERATED PROTONS

Mircea PĂTRĂŞCOIU[*1,2], Lucian TUDOR[1], Bogdan DIACONESCU[1], Dan Gabriel GHIŢĂ[1], Grigore Octavian DONŢU[3], Cătălin M. TICOŞ[1,2]

A particle steering system is proposed based on dipoles and quadrupoles to steer, transport and focus protons with energies between 70-130 MeV produced by a laser plasma accelerator. The proton beam is simulated by using SIMION ion optics software taking a point-like source and a divergent beam of 4 degrees. For the energy spectrum of the beam, two cases were considered: a uniform distribution and a decaying exponential one towards the highest energies. The full length of the system from source to the last detector is 3.8 m The setup shows good focusing capabilities, bunching most of the particles in a 25×15 *mm*^{2} *area with a 60% efficiency on the detection screen in the case of the uniform distribution. This paired with the high energy particles used in the simulation could prove to be an effective way of focusing protons beams for multiple applications, such as their use in radiotherapy.*

Keywords: Dipole magnet, quadrupole magnet, proton beam, particle beam steering, numerical simulations

1. Introduction

Laser driven particle acceleration has been intensively investigated in the last two decades as a more compact and accessible way of particle acceleration. There are different acceleration techniques for ions and electrons, which generally involve the use of different targets and a high-power laser focused in a small spot, of a few microns in diameters, on the target. In the case of protons, the most studied mechanism is the Target Normal Sheath Acceleration (TNSA) which is based on the strong electric fields created at the rear side of a thin film upon ionization and expulsion of electrons by laser irradiation [1]. In spite that the targets can be made of different materials (e.g. Al., Au, Ni, etc.) the source of protons is from the adsorbed water layer from the residual vacuum found on the target surface. TNSA

[*] Corresponding author
[1] Horia Hulubei National Institute for R&D in Physics and Nuclear Engineering, Extreme Light Infrastructure - Nuclear Physics (ELI-NP), Măgurele, 077125, ILFOV county, Romania,
[2] Engineering and Applications of Lasers and Accelerators Doctoral School (SDIALA), National University of Science and Technology POLITEHNICA of Bucharest, Bucharest, Romania
[3] Department of Mechatronics and Precision Mechanics, National University of Science and Technology POLITEHNICA of Bucharest, Bucharest, Romania

requires laser intensities of at least 10^{18} Wcm^{-2} and targets with a thickness of a few microns. Other mechanisms are being explored as higher laser intensities (i.e. $I = 10^{23}$ Wcm^{-2}) have become accessible with lasers reaching a peak power of several PW. The Radiation Pressure Acceleration (RPA) is an example in which an ultrathin foil (with width of tens of nanometer) is fully ionized and both electrons and ions are accelerated altogether as a result of the light pressure pushing the electrons [2]. The Breakout Afterburner (BOA) is another mechanism in which the ionized target becomes relativistically transparent to the laser light allowing an additional heating of the electrons which drive the ions to a higher energy [3]. There is also a hybrid acceleration regime which includes features from both TNSA and RPA, at laser intensities somewhat intermediate towards attaining a full RPA regime. The maximum proton energy reported so far is in the range 90 to 150 MeV [4,5].

The resulting proton beams can have different applications in radiography, fusion and radiotherapy [3]. Several limitations prevent at the current stage to use the laser-accelerated ions in medical applications: the large beam divergence, the low charge and the large dispersion of energy in the particles. There are also advantages stemming from the short duration of the laser pulse which make possible dose rates over 40 Gys-1 in the FLASH regime [6]

In this paper we simulate the transport and focusing of proton beams with energies between 70 and 130 MeV, high enough to be considered for a relatively shallow seated tumor treatment, while the required range for a deeper penetration would be around 250 MeV. Particle beam steering systems play a crucial role in various scientific and industrial applications, including particle accelerators, medical radiation therapy, and electron microscopy [7-12]. These systems enable precise control over the trajectory of charged particle beams ensuring their direct manipulation as needed. Among the key components employed in particle beam steering systems are dipole and quadrupole magnets, which utilize electromagnetic fields to bend and focus the particle beams [5][6].

Dipole magnets are fundamental elements in particle beam steering systems, consisting of a pair of magnets arranged to create a uniform magnetic field in a single direction across the gap between their poles. [7-10]. When a charged particle beam passes through a dipole magnet, it experiences a force perpendicular to its initial trajectory due to the Lorentz force. This force causes the particle beam to bend along a curved path [9]. The strength of the magnetic field produced by a dipole magnet is a critical factor in determining the degree of bending. The higher the magnetic field strength, the greater the deflection of the charged particles. By adjusting the strength of the magnetic field, scientists can precisely steer the particle beam to follow the desired trajectory [10]. The bending radius of a particle trajectory is

$$B\rho = \frac{pc}{q} \tag{1}$$

where B is the strength of the magnetic field in tesla (T), p is the particle momentum, c being the speed of light in vacuum, and q is the charge of the particles, protons in this case. As an example, for $B = 1$ T we get for 70 MeV protons a bending radius of 0.18 m, for 100 MeV protons it is 0.26 m while for 130 MeV protons it is 0.33 m.

Unlike dipole magnets, quadrupole magnets consist of four magnets arranged in a specific configuration. Two of the opposite magnets have a magnetic field pointing inwards, while the other two have a field pointing outwards. This arrangement forms what is known as a quadrupole field [10]. The quadrupole field focuses the particle beam by exerting forces that vary linearly with displacement from the ideal beam trajectory. The horizontal focusing forces pull the particles toward the center, while the vertical focusing forces push them back to the central plane. By properly adjusting the strength and configuration of the quadrupole magnets, a tightly focused beam, can be achieved [11]. The combined use of dipole and quadrupole magnets in a particle beam steering system allows for precise control over both the trajectory and focus of the beam. By strategically arranging these magnets along the beamline, complex beam paths and fine adjustments of the beam's characteristics can be achieved [11].

Advancements in particle beam steering systems using dipole and quadrupole magnets have significantly contributed to various scientific fields. In high-energy physics, these systems are crucial in providing beam steering capability needed in building high energy particle accelerators, thus allowing to study the fundamental properties of matter [7-10]. They are also essential in medical radiation therapy, where precise control over the beam's trajectory and focus is vital to targeting tumors while minimizing damage to healthy tissue [13].

2. Simulations setup

Below, the design and 3D simulation setup of such a system used for protons with energies between 70 and 130 MeV is presented. A sketch of the beam transport is presented in Fig. 1. For this simulation, a point-like source generating 5000 protons is used, with two types of energy distributions. In the first case a flat energy distribution is considered over the full range from 70 to 130 MeV. In the second case an exponential distribution with decaying number of protons towards higher energies is considered. This is intended to mimic the beam of protons emitted from the interaction of a high-power laser with a thin foil. The emitted beam has a cone-like shape with an angular divergence of 4 degrees.

The beam is first steered using a pair of dipoles, after which it is passed through a round aperture which acts as a spatial filter. This ensures that the beam profile is able to fit through the centre of two pairs of quadrupoles. The beam diameter in cross section is tuned in order for it to avoid touching the magnets of the quadrupoles, by varying the filter position. Irradiation of the magnets with protons can produce structural damages and demagnetization.

The dipoles are 400 mm in length with a 1.3 T magnetic field strength and a gap of 138mm between the poles. The spatial particle filter has a diameter of 80 mm while the quadrupoles used are 100 mm in length, with a 100 mm gap between the poles. The strength of the quadrupoles at the tip is 1.8 T, identical for all of them. To determine the gradient of the quadrupole the following formula is used:

$$G = \frac{B}{r} \quad (2)$$

where B is the magnetic field strength at the pole tip and r is the aperture radius. With an aperture of 50 mm a gradient of 36 T/m is obtained. The sequence of the quadrupole doublets used in this simulation is focusing – defocusing (FODO). Along the beam a slot shaped filter followed by a transversal screen are placed at some distance to detect the position of the protons.

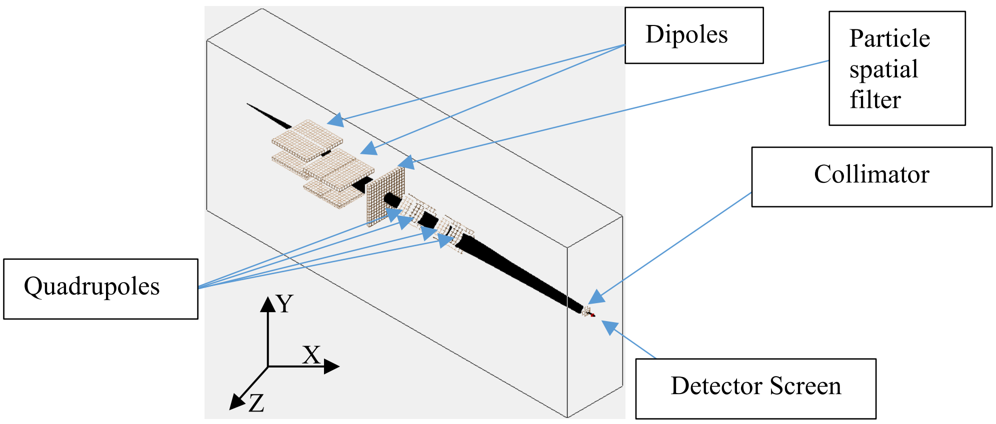

Fig. 1 3D overview of the full particle beam steering system which comprises the pair of dipoles, a spatial filter, the 2 pairs of quadrupoles, a slot shaped filter and a detection screen.

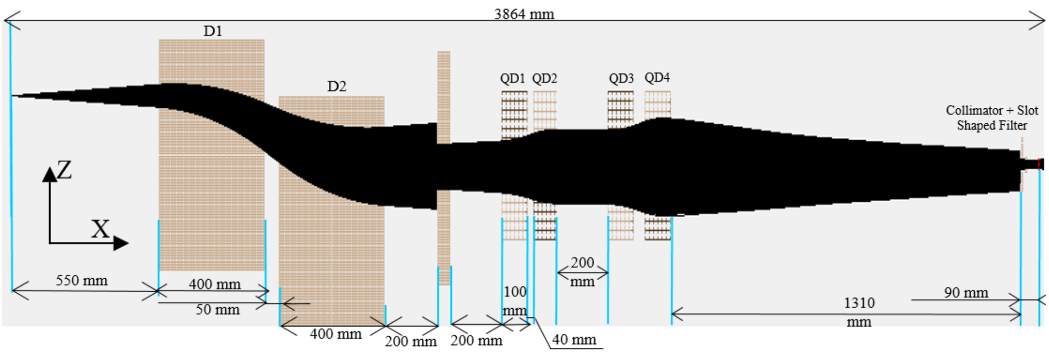

Fig. 2 – Top view of the steering system showing the two dipoles D1 and D2 followed by the particle filter (400x400x50 mm), the 2 sets of quadrupoles: QD1 (100 mm), QD2, QD3 and QD4 the collimator (100x100x20) and the slot shaped filter (30x30x10 mm).

The first dipole D1 is placed 550 mm from the particle source, as shown in Fig. 2. The second one is 50 mm away with a 100 mm gradient difference on the Z axis. The first spatial filter is 200 mm away from the second dipole. The first quadrupole is 200 mm away from the first filter. Then the next elements can be viewed as a lattice which consists of 2 quadrupole doublets, ending with a collimator and a slot shaped filter. The total length of the setup, from the particle source to the detector screen is 3864 mm, making it feasible.

3. Results

In the first case of a setup which does not include the last collimator and slot shaped filter, a total of 3262 particles are recorded on the detection screen resulting in more than 60% ratio of transported particles. After introducing the last collimator, which has a diameter of 20 mm, and filter, which has has a slot shape of 13 mm in length and 4 mm in height, approximately 23% or 1150 particles (70-100 MeV) are detected.

As the particles are emitted from the source, they are first bent, depending on their velocity, by the first dipole and then steered again by the second one to compensate the gradient and regain the intended trajectory. A benefit of this manipulation, is the fact that the dipoles naturally induce a very small amount of focusing into the beam due to the fringe fields or edge focusing. After the particles pass through the second dipole and regain their initial trajectory, they go through a spatial filter which profiles the beam into a round shape, at the cost of particle counts, in order to better pass through the quadrupoles. Inside the quadrupoles, the beam experiences focusing and defocusing depending on the orientation of the magnets thus achieving an overall focusing effect decreasing the emittance of the beam. Once the particles go through both quadrupole doublets, they again pass through an additional collimator and filter, further profiling ensuring the main bunch of the particles are passing through to the detection screen. The role use of the last collimator and slot shaped filter is to allow for a precise energy selection. Since the particles have different trajectories depending on their energy, these last 2 components can be adjusted depending on the energy that is desired on the detection screen. An example of the spatial distribution of the particles is shown in Fig. 3. The particles are distributed over an area of approximately 60 mm (OZ) × 50mm (OY) with the main bulk of the particles being in an area of approximately 25mm (Z) × 15mm (Y). It is a significant improvement over the 80mm diameter beam which enters the quadrupoles.

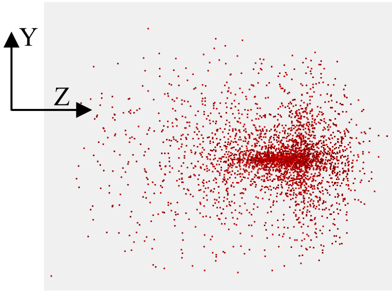

Fig. 3 Particle distribution on the detection screen with scale

The spatial distribution is slightly off-center because the quadrupole induces a dipolar effect on the particles meaning that they do not only focus the beam but at the same time they also steer it slightly. This is caused by the multipole errors of magnets. In order to correct this, there is the possibility of adding corrector magnets (dipoles) which can be adjusted according to the deviation of the beam in order to keep it centered on the detection screen. This is however in the initial case, when no the additional collimator and filter are introduced at the end of the beam.

Fig. 4 shows a comparison between three different setups, one without any collimator or filter before the detection screen (A), one with just a collimator (B) and one with both a collimator and a slot shaped filter (C). It can be observed that, in the first case, the energy distribution remains relatively flat, indicating the system's capability to transport protons with energies between 70 and 130 MeV at a consistent level. This allows for an energy selection improvement using movable collimators and filters. As observed in the second and third cases, the energy profile becomes more defined. This suggests that the current placement of the collimators in the simulation allows more particles with energies between 80-85 MeV to pass through. If their position would be adjusted, the energy profile of the beam on the detection screen would change. One downside of this setup is that in order to perform this type of selection, for each element added, there is a loss of particles that occurs as seen in the total counts of the particles. From no collimator to 1 collimator there is a loss of approximately 1000 particles and an additional 10^3 from the collimator to the slot shaped filter, in total meaning a capture rate of 25% from the initial 5000 particles. This however can be offset depending on the energy spread of the particles resulting from the experiment.

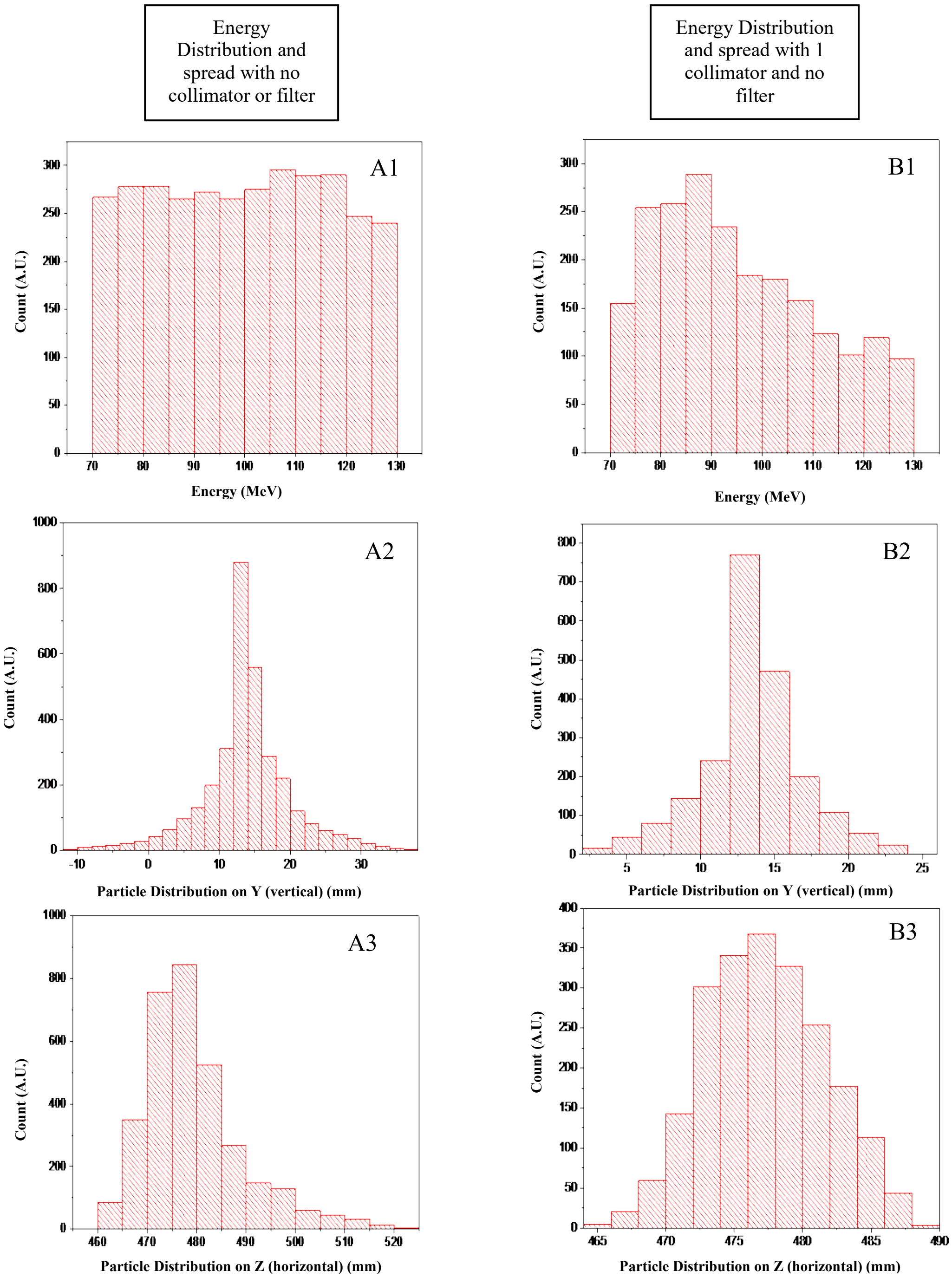
Energy Distribution and spread with no collimator or filter
Energy Distribution and spread with 1 collimator and no filter
A1
Count (A.U.)
Energy (MeV)
B1
Count (A.U.)
Energy (MeV)
A2
Count (A.U.)
Particle Distribution on Y (vertical) (mm)
B2
Count (A.U.)
Particle Distribution on Y (vertical) (mm)
A3
Count (A.U.)
Particle Distribution on Z (horizontal) (mm)
B3
Count (A.U.)
Particle Distribution on Z (horizontal) (mm)

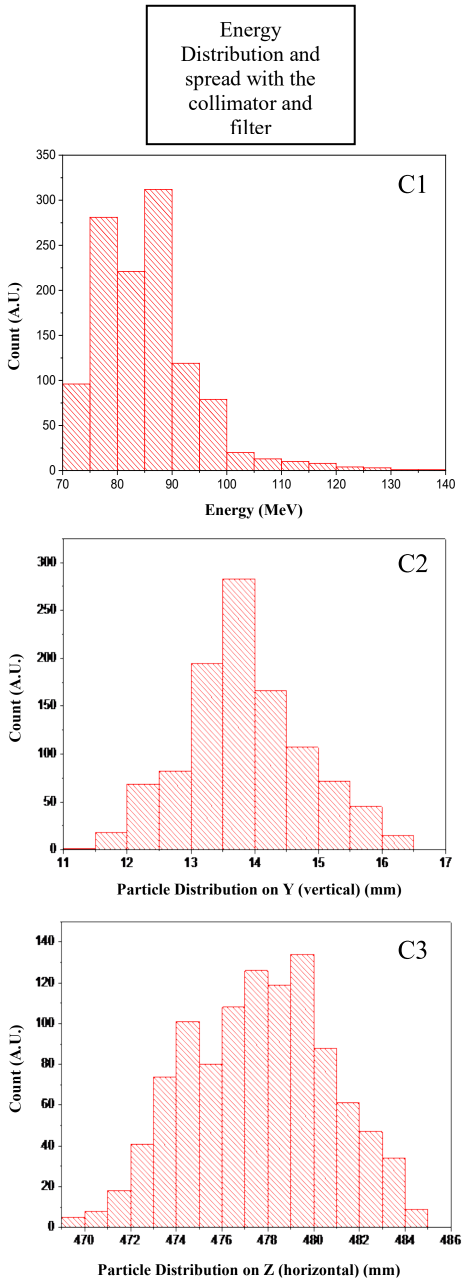

Fig. 4 – Comparison between setups using: no collimator or filter (A1, A2, A3), 1 collimator (B1, B2, B3), both collimator and slot shaped filter (C1, C2, C3)

In the followings we can see the energy spread of the particles on the detection screen when using a more realistic energy distribution for a laser-target interaction with the TNSA acceleration regime. The distribution of energy is exponentially decaying. It can be observed that in this case, most of the particles resulted from the interaction are taken in the range 75 to 90 MeV. This further proves the focusing and energy selection capabilities of the setup if the parameters are slightly adjusted. For example, if the dipoles get a magnetic field increase or decrease, there will be a different spot on the detection screen where the particles land. If the collimators are adjusted accordingly, only the particles with a selected range of energies will pass through, a feature that could make possible its use in hadron therapy where a very precise dose and energy are required.

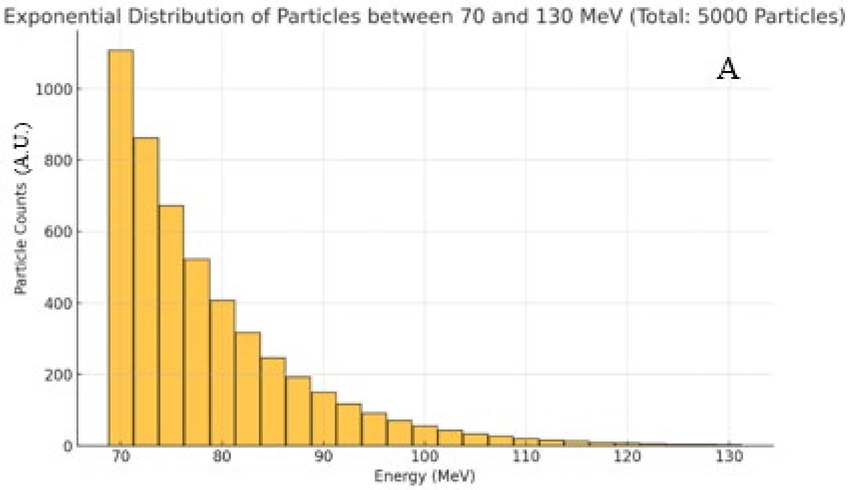

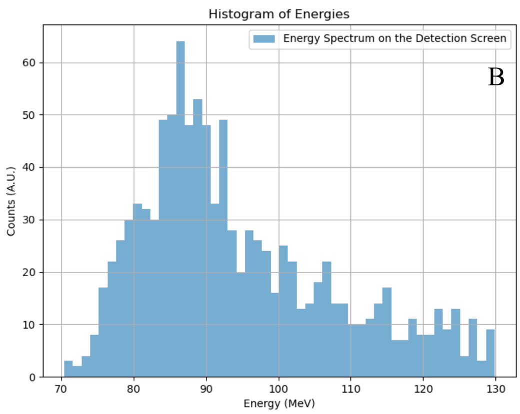

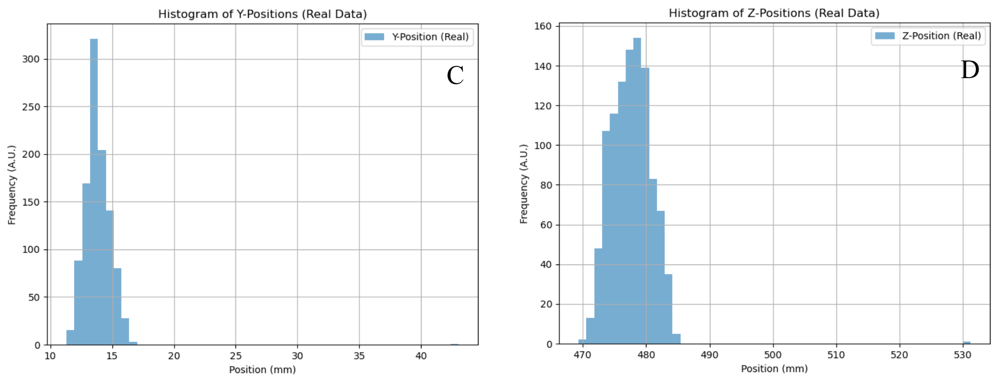

Fig. 5 – Energy distribution of particles (B) as well as positions on the screen (C,D), using an exponential distribution (A) assumed to result from a TNSA acceleration regime with a filter and collimator

In a real experiment the total proton number emitted from the target during a shot is in the range of 10^{11} - 10^{13}. In our case a much lower number of particles is simulated. And for this reason the results presented in Fig. 6 show a somewhat distorted result, especially in the phase space domain. The calculated beam emittance for the real data is on OY axis $\varepsilon_Y = 2.08 \times 10^{-6}$ mm·mrad and on the OZ-axis: $\varepsilon_Z = 7.25 \times 10^{-6}$ mm·mrad.

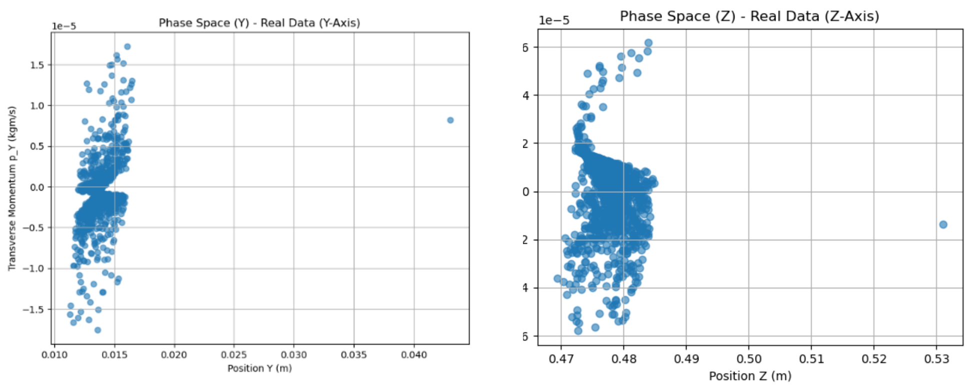

Fig.6 Phase space of the proton beam in the Y and Z planes.

The outliers that are seen in the graphs are due to straggling particles that were overshot and thus passed above the filter. This is an issue that is easily solved by adjusting the dimension of the filters in a real case application. As a way to overcome the limitation of the simulation and compare the results to a more realistic case, the output of the data set in the simulation was increased from 1150 particles to 100000 particles by injecting artificial particles following the spatial distribution shown in Fig. 5. Basically, this can allow the observation of the behavior of more particles with the same characteristics, as shown in Fig. 7. For the expanded data set the new emittances are on the Y-axis $\boldsymbol{\varepsilon_Y = 3.88} \times \mathbf{10^{-6}}$ mm·mrad and on the OZ-axis: $\boldsymbol{\varepsilon_Z = 3.5} \times \mathbf{10^{-6}}$ mm·mrad.

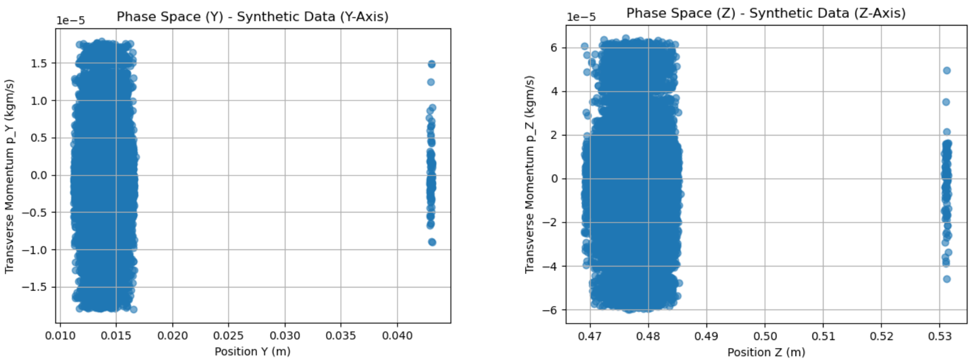

Fig. 7 – Phase space for the expanded data set.

From the synthetic data we can observe that the particles start taking the shape of the slot shaped filter. These results provide more insight into how the setup should behave in a more realistic scenario even if the number of simulated particles is much lower than in the real case. This further supports the medical use case scenario where such a distribution of particles could be used in hadron therapy by making use of the last filter and collimator which are adjustable. The large energy distribution of the particles due to intrinsically acceleration mechanism can be advantageous as it can accommodate the entire Bragg peak spectrum of the particles bombarding simultaneously the full extension of the tumor, and providing a more efficient and faster treatment plan.

3. Conclusions

In conclusion, particle beam steering systems, utilizing dipole and quadrupole magnets, provide precise control over the trajectory and focusing of charged particle beams. Dipole magnets are responsible for bending the beam path, while quadrupole magnets handle its focusing and collimation. By combining these two types of magnetic systems, effective steering of particle beams generated by laser-plasma accelerators is achieved. The results presented in this work are encouraging and offer valuable insights for designing advanced systems, potentially applicable to the radiation treatment of deep-seated tumors.

In the studied setup, the proton beam exhibits an energy spectrum ranging from 70 to 130 MeV, with two distinct energy distributions: flat and exponentially decaying. The beam also has a divergence angle of 4 degrees. Under these conditions, the majority of protons are concentrated within a 16 × 13 mm² area at a distance of approximately 3.8 meters, demonstrating excellent targeting capabilities.

A particularly intriguing aspect is the Bragg peak of protons and their interaction with matter. Unlike traditional particle accelerators, where chromaticity poses significant challenges, laser-based hadron therapy can exploit these effects to its advantage. Consequently, it is feasible to construct a simple yet robust magnet lattice capable of reliably delivering particles from the source, high-power laser interacting with a target, to a detector screen, which, in future applications, could be a patient.

Acknowledgements

This work was supported by the PN 23 21 01 05 contract funded by the Romanian Ministry of Research, Innovation and Digitalization (MCID), the IOSIN funds for research infrastructures of national interest and project ELI-RO-19 HighProtonPlas funded by IFA.

R E F E R E N C E S

[1] *Roth M, Schollmeier M.* Ion Acceleration—Target normal Sheath Acceleration. In: B Holzer, editor. Proceedings of the CAS-CERN Accelerator School: Plasma Wake Acceleration; 23–29 November 2014; Geneva, Switzerland. SPIE (2016).

[2] *Qiao B. et al.,* Dominance of Radiation Pressure in Ion Acceleration with Linearly Polarized Pulses at Intensities of 10^{21} Wcm^{-2}, Phys. Rev. Lett. 108, 115002 (2012).

[3] *Fernandez J. C. et al.,* Laser-plasmas in the relativistic-transparency regime: Science and applications, Phs. Plasmas 24, 056702 (2017).

[4] *Higginson A. et al.,* Near-100 MeV protons via a laser-driven transparency-enhanced hybrid acceleration scheme, Nat. Commun. 9, 724 (2018)

[5]. *Ziegler T et al.* Laser-driven high-energy proton beams from cascaded acceleration regimes. Nature Physics 20, 1211 (2024)

[6] *Kim M.M. et al*., Development of Ultra-High Dose-Rate (FLASH) Particle Therapy, IEEE Trans. Rad. Plasma Med. Sci.,6, 252 (2022).

[7]. *Smith, J.*, Particle Beam Steering in Accelerators, Journal of Physics: Conference Series, 2019.

[8]. *Brown, R.*, Beam Steering in Medical Linear Accelerators, Journal of Applied Clinical Medical Physics, 2020.

[9]. *Wiedemann, H.*, Particle Accelerator Physics: An Introduction, Springer Science & Business Media, 2007.

[10]. *Wilson, E. J. N.*, An Introduction to Particle Accelerators, Oxford University Press, 2013.

[11]. *Chao, A. W.*, Handbook of Accelerator Physics and Engineering, World Scientific Publishing, 2013.

[12]. *Spence, J. C. H.*, Experimental High-Resolution Electron Microscopy, Oxford University Press, 2013.

[13]. *Mohan, R.*, Principles and Practice of Radiation Therapy, Lippincott Williams & Wilkins, 2015.